Time-dependent density-functional study of the ionization and fragmentation of C_{2}H_{2} and H_{2} by strong circularly polarized laser pulses

Arthur Russakoff and Kálmán Varga

Phys. Rev. A **92**, 053413 — Published 9 November 2015

DOI: 10.1103/PhysRevA.92.053413

Time-dependent density functional study of the ionization and fragmentation of C_2H_2 and H_2 by strong circular polarized laser pulses

Arthur Russakoff[1] and Kálmán Varga[1]

[1] *Department of Physics and Astronomy, Vanderbilt University, Nashville, Tennessee 37235, USA*

The ionization and fragmentation dynamics of acetylene and the hydrogen molecule driven by strong short circularly polarized laser pulses are investigated within the framework of the Time–Dependent Density Functional Theory coupled with the Ehrenfest dynamics. The effects of alignment are considered and the dynamics are compared to that driven by linearly polarized pulses. It is found that the coupled ion-electron dynamics of both molecules driven by circularly polarized pulses follow the enhanced ionization mechanism, as was found in previous theoretical studies with linearly polarized pulses. A moderate localization asymmetry in the ionization dynamics of the hydrogen molecule was also found, in qualitative agreement with previous experimental investigations.

I. INTRODUCTION

The interaction of molecules with strong short laser fields involves the complex coupled dynamics of fast moving electrons and slow moving nuclei[1–6]. There are many important applications for strong short pulses, e.g. ultrafast imaging[7, 8], high–harmonic generation[9–11], and quantum control[12–14]. Of particular interest is multi-electron ionization, the simplest case being double ionization. Double ionization may be broadly divided into two categories: sequential[15, 16] and nonsequential[17–21]. For sequential double ionization (SDI) each electron is ejected one at a time, a process well described by the single-active-electron model [22–25]. In nonsequential double ionization both electrons are ejected simultaneously, and the electron dynamics are therefore highly correlated[26].

For a linearly polarized laser pulse, the dominant mechanism for nonsequential double ionization is that of electron recollision, where first an electron is ionized and then upon reversal of the field the electron is driven back to the parent molecule where the recollision leads to excitation or ionization of a second electron [27, 28].

Previously it was expected that in a circularly polarized laser field the recollision processes would be suppressed since there is no reversal of the laser field. Xie et al. [29] experimentally observed the CH_2^+/H^+ fragmentation channel of acetylene (C_2H_2) induced by either a linearly or circularly polarized laser pulse pulses. It was found that H^+ ion kinetic energies greater than 4.5 eV were suppressed for the circularly polarized pulse, despite its similar intensity and duration to the linearly polarized pulse. This was attributed to the suppression of nonsequential double ionization events such as recollision.

On the other hand, Non-Sequential Double Ionization (NSDI) events have been experimentally observed for the molecules NO and O_2 subjected to circularly polarized pulses[30]. Theoretically, Tong et al.[31] used a classical ensemble approach to show that NSDI occurs for H_2 driven by a circularly polarized pulse. Furthermore, they showed that the NSDI is due to a recollision process where an electron localized at one ion site is driven along an elliptical path to the other ion site. The first electron then collides with and ionizes the second electron. This recollision process becomes more probable for extended molecular geometries. Yuan et al.[11] solved the two-dimensional time-dependent Schrodinger equation for H_2^+ and showed that recollision electron dynamics with extended molecular geometries may also be used in the generation of high-order elliptically polarized harmonics.

In addition to the dependence on bond length, the ionization of molecules is also dependent on the alignment of the molecule relative to the polarization vector. For a linear molecule, the alignment is uniquely determined by the angle between the molecular axis and the laser's polarization vector. Ionization is maximized when this angle is zero[32, 33]. In a circularly polarized laser field, angular streaking deflects the ionized electron. This angular streaking occurs since the Coulomb potential produced by the nuclei of the molecule is not spherically symmetric[34]. If the tunneling ionization time is instantaneous and the initial electron momentum is zero, then the circularly polarized field deflects the ionized electron by 90°. Hence for linear molecules, the peak of a measured photoelectron spectrum is typically perpendicular to the molecular axis[35, 36]. However, measurements of the ionization H_2^+ give peak ionization angles between 15° and 45°[37, 38], implying a more complex electron dynamics.

Bandrauk et al.[39] considered the effects of the enhanced ionization of H_2^+ driven by a circularly polarized pulse with polarization vector always perpendicular to the molecular axis. By solving the 3D Schrodinger equation for various extended bond lengths, they obtained ionization rates as a function of bond length. They found that the ionization rate increases and then plateaus as the bond length is increased.

In this manuscript we present an in depth investigation of the coupled ionization and fragmentation dynamics of H_2 and C_2H_2 driven by circularly polarized strong laser fields by performing Time-Dependent Density Functional Theory (TDDFT) calculations coupled with the Ehrenfest dynamics. We consider various intensities and pulse durations typical in experiment[5, 29], two different alignments, and compare the dynamics driven by a circularly polarized pulse to linearly polarized pulses of similar strength.

In section II we shall discuss the computational details of the TDDFT simulations, and in section III we describe the results of the simulations, and in section IV we give a short discussion comparing our results with previous theoretical and experimental investigations.

II. COMPUTATIONAL DETAILS

The electron dynamics in the simulations were modeled using Time Dependent Density Functional Theory (TDDFT)[40] on a real–space grid with real–time propagation. Core electrons, which are difficult to handle computationally, were represented using norm-conserving Troullier-Martins pseudopotentials [41].

At the beginning of the TDDFT calculations the ground state of the system is prepared by performing a density functional theory calculation. Next, the time–dependent Kohn–Sham orbitals, $\psi_k(\mathrm{r}, t)$, are determined by solving the time–dependent Kohn–Sham equation

$$i\hbar\frac{\partial\psi_k(\mathbf{r},t)}{\partial t} = H\psi_k(\mathbf{r},t), \tag{1}$$

where k is a quantum number labelling the orbital. The Hamiltonian above is given by

$$H = -\frac{\hbar^2}{2m}\nabla^2_{\mathbf{r}} + V_{\mathrm{H}}[\rho](\mathbf{r},t) + V_{\mathrm{XC}}[\rho](\mathbf{r},t) + V_{\mathrm{ext}}(\mathbf{r},t). \quad (2)$$

Here ρ denotes the electron density, which is defined by a sum over all occupied orbitals:

$$\rho(\mathbf{r},t) = \sum_{k=1}^{\infty} 2|\psi_k(\mathbf{r},t)|^2, \quad (3)$$

where the factor of 2 accounts for there being two electrons in each orbital (via spin degeneracy).

V_{H} in eq. 2 is the Hartree potential, defined by

$$V_{\mathrm{H}}(\mathbf{r},t) = \int d\mathbf{r}' \frac{\rho(\mathbf{r}',t)}{|\mathbf{r}-\mathbf{r}'|}, \quad (4)$$

and accounts for the electrostatic Coulomb interactions between electrons. V_{XC} is the exchange–correlation potential, whose exact form is a complicated functional of the entire history of the electron density. This functional was approximated use the adiabatic local–density approximation (ALDA) with the parameterization of Perdew and Zunger [42]. The last term in eq. 2, V_{ext}, is the external potential, which includes the implicitly time–dependent potential due to the ions, V_{ion}, and the explicitly time–dependent potential due to the electric field of the laser V_{laser}. V_{ion} is a sum of norm-conserving pseudopotentials of the form given by Troullier and Martins [41] centered at each ion.

V_{laser} is described using the dipole approximation, $V_{\mathrm{laser}} = \mathbf{r}\cdot\mathbf{E}(t)$, with the time–dependent circularly polarized electric field given by,

$$\mathbf{E}(t) = E_{\max}\exp\left[-\frac{(t-t_0)^2}{2a^2}\right]\left(\hat{\mathbf{k_1}}\sin(\omega t) + \hat{\mathbf{k_2}}\sin(\omega t + \frac{\pi}{2})\right). \quad (5)$$

The parameters a, t_0, and $E_{\max}$ define the width, initial position of the center, and the maximum amplitude of the Gaussian envelope, respectively. ω describes the frequency of the laser. $\hat{\mathbf{k_1}}$ and $\hat{\mathbf{k_2}}$ are orthogonal unit vectors defining the polarization electric field.

In our calculations, the time–dependent orbitals are propagated using a fourth-order Taylor expansion of the propagator, so that the propagation of the Kohn-Sham orbitals over a very short time step, δt, is given by,

$$\psi_k(\mathbf{r}, t_q + \delta t) \approx \sum_{n=0}^{4}\frac{1}{n!}\left(-\frac{i\delta t}{\hbar}H(\mathbf{r},t_q)\right)^n \psi_k(\mathbf{r},t_q). \quad (6)$$

The operator is applied for N time steps until the final time, $t_{\mathrm{final}} = N\cdot\delta t$, is obtained. While the Taylor–propagation is not unconditionally stable, for time steps chosen to suitably small the propagation is very stable. The advantage of the Taylor-propagation is that its simple form only requires the repeated action of the Hamiltonian on the wave function. A review and comparison of the advantages and disadvantages of different time propagating schemes in TDDFT can be found in Ref. [43].

In real space TDDFT the Kohn-Sham orbitals are represented at discrete points in real space. In practice these discrete points are organized in a uniform rectangular grid, and the accuracy of the simulations are controlled by adjusting a single parameter: the grid spacing. At the walls of the simulation cell we enforce the boundary condition that the Kohn–Sham orbitals are zero at the walls. When a strong laser field is applied, ioniation may occur and the zero–boundary condition can lead to an unphysical reflection of the wavefunction off the walls of the simulation cell. To prevent this we implemented a complex absorbing potential (CAP) with the following form, given by Manolopoulos [44]:

$$-iw(x) = -i\frac{\hbar^2}{2m}\left(\frac{2\pi}{\Delta x}\right)^2 f(y) \quad (7)$$

where x_1 is the start and x_2 is the end of the absorbing region, $\Delta x = x_2 - x_1$, $c = 2.62$ is a numerical constant, m is the electron's mass and

$$f(y) = \frac{4}{c^2}\left(\frac{1}{(1+y)^2} + \frac{1}{(1-y)^2} - 2\right), \quad y = \frac{(x-x_1)}{\Delta x}. \quad (8)$$

As the molecule is ionized by the laser field, electron density will travel to the edge of the simulation box where it is absorbed by the CAP. The total electron number,

$$N(t) = \int_V \rho(\mathbf{r},t)d^3x, \quad (9)$$

where V is the volume of the simulation box, will therefore diverge from the initial electron number, $N(0)$. We interpret $N(0) - N(t)$ as the total ionization of the molecule.

Motion of the ions in the simulations were treated classically. Using the Ehrenfest theorem [45], the quantum forces on the ions due to the electrons are given by the derivatives of the expectation value of the total electronic energy with respect to the ionic positions. These forces are then fed into Newton's Second Law, giving

$$M_i\frac{d^2\mathbf{R}_i}{dt^2} = Z_i\mathbf{E}_{\mathrm{laser}}(t) + \sum_{j\neq i}^{N_{\mathrm{ions}}}\frac{Z_iZ_j(\mathbf{R}_i-\mathbf{R}_j)}{|\mathbf{R}_i-\mathbf{R}_j|^3} - \boldsymbol{\nabla}_{\mathbf{R}_i}\int V_{\mathrm{ion}}(\mathbf{r},\mathbf{R}_i)\rho(\mathbf{r},t)d\mathbf{r}, \quad (10)$$

where M_i and Z_i are the mass and pseudocharge (valence) of the i-th ion, respectively, and N_{ions} is the total number of ions.

The computational results presented in the next section use the following parameters. The rectangular box

is given by $L_x = L_y = L_z = 34$ Å. The molecular axis lies in the x direction. The grid spacing is 0.25 Å in each direction. The CAP is nonzero in a region 5 Å from the walls of the simulation cell. The time step for the propagation of the wave function is $\delta t = 0.0007$ fs. The equation of the ionic motion (eq. 10) is solved with the Verlet algorithm with time step 0.0028 fs. These parameters lead to very well converged results. The calculated ionization potential is 11.8 eV for C_2H_2, comparable with the experimental value 11.4 eV [46].

III. RESULTS

A. H_2

In this section we present the simulation results for the H_2 molecule. In the first subsection the molecular axis is aligned parallel to one of the circularly polarized pulse's polarization vectors, and in the following subsection the molecular axis is perpendicular to both of the circularly polarized pulse's polarization vectors.

1. *Polarization vectors along the x and y axes*

Columns (1-2) of Fig. 1 show the ionization and fragmentation of an H_2 molecule driven by circularly polarized laser pulse whose polarization vectors, $\hat{\mathbf{k_1}}$ and $\hat{\mathbf{k_2}}$, lie along the x and y axes respectively (see eq. 5). The linear molecule initially lies along the x axis. Two laser intensities, and $4 \cdot 10^{14}$ and $14 \cdot 10^{14} \frac{\mathrm{W}}{\mathrm{cm}^2}$, and two full width half maximum (FWHM) pulse widths, 4.5 and 25 fs, were considered for a total of four laser pulses. The wavelength of all considered pulses is 790 nm. We also compare these results to two separate simulations where the dynamics are driven by linearly polarized pulses of the same intensity and pulse width. We consider linear polarizations aligned along either the x or y axis.

As shown in Fig. 1.a, a circularly polarized laser pulse of intensity $4 \cdot 10^{14} \frac{\mathrm{W}}{\mathrm{cm}^2}$ and pulse width 4.5 fs, ionizes the molecule by 0.63 electron. The pulse is too weak to break the H-H bond, and only a small oscillation is observed (see Fig. 1.b). The Ehrenfest dynamics represent an averaging of the possible fragmentation channels, and the lack of bond breaking implies that the probability of fragmentation is small. A linearly polarized pulse with polarization vector aligned along the x axis ionizes 0.38 electrons, and one aligned along the y axis ionizes 0.32 electron. Since the circularly polarized pulse is simply the sum of two orthogonal linearly polarized pulses with phase shift $\frac{\pi}{2}$, one asks if the ionization is simply the sum of ionization from the two separate linearly polarized pulses. In this case, the ionization driven by the circularly polarized pulse is somewhat smaller than the sum of the individual linear components.

At first glance, the simulations with linearly polarized pulses seem to imply that the ionization rate induced by the circularly polarized pulse will be greater along the x axis than along the y axis. While the strongest ionization does occur when the polarization vector of the pulse is aligned with the x axis, angular streaking will occur and the peak in the photoelectron spectrum will be at some angle relative to the x axis[34–38].

In Fig. 1.e, the intensity is $4 \cdot 10^{14} \frac{\mathrm{W}}{\mathrm{cm}^2}$ and pulse width is 25 fs. The circularly polaried pulse induces an ionization of 1.90 electrons. This large ionization causes a Coulomb explosion and the two H^+ ions move apart with trajectories that lie essentially along the x axis (see Fig. 1.f). The corresponding parallel and perpendicular linearly polarized pulses induce an ionization of 0.90 and 0.68 electron, respectively. Unlike the previous laser parameters, the sum of the ionization induced by the two separate linear pulses, 1.58 electrons, is smaller than the ionization induced by the circularly polarized pulse. The key difference between the linearly and circularly polarized pulses here is that the linearly polarized pulses do not induce a Coulomb explosion. As the H-H bond length increases the ionization efficiency also increases, a mechanism known as enhanced ionization. Since the enhanced ionization mechanism occurs for the circularly polarized pulse, its ionization is much more efficient than either of its linear components alone.

At an intensity of $14 \cdot 10^{14} \frac{\mathrm{W}}{\mathrm{cm}^2}$ and a pulse width of 4.5 fs, the circularly polarized pulse and two linearly polarized pulses all induce Coulomb explosion (see Fig. 1.j). Enhanced ionization occurs for all three pulses and the ionization induced by each of the two linearly polarized pulses, 1.58 and 1.28 electrons for the x and y alignments respectively, sum to greatly exceed the ionization of the circularly polarized pulse, which is 1.97 electrons (see Fig. 1.i).

At an intensity of $14 \cdot 10^{14} \frac{\mathrm{W}}{\mathrm{cm}^2}$ and pulse width of 25 fs, the linearly and the circularly polarized pulses all have sufficient strength to ionize the molecule completely (Fig. 1.m). The rate of ionization for the circularly polarized pulse is somewhat higher. All three pulses induce Coulomb explosion (see Fig. 1.n). Typically, the fragmentation dynamics drive H^+ ions along the x axis. However, at this particular intensity and duration the circularly polarized pulse induces a small but non-negligible motion in the y axis. This y axis is not observed for the linearly polarized pulses even when the polarization vector lies along the y axis.

2. *Polarization vectors along the y and z axes*

Columns 3 and 4 of Fig. 1 show the ionization and fragmentation dynamics when the laser pulse's polarization vectors, $\hat{\mathbf{k_1}}$ and $\hat{\mathbf{k_2}}$, lie along the z and y axes respectively (see eq. 5). We only consider linear polarization aligned

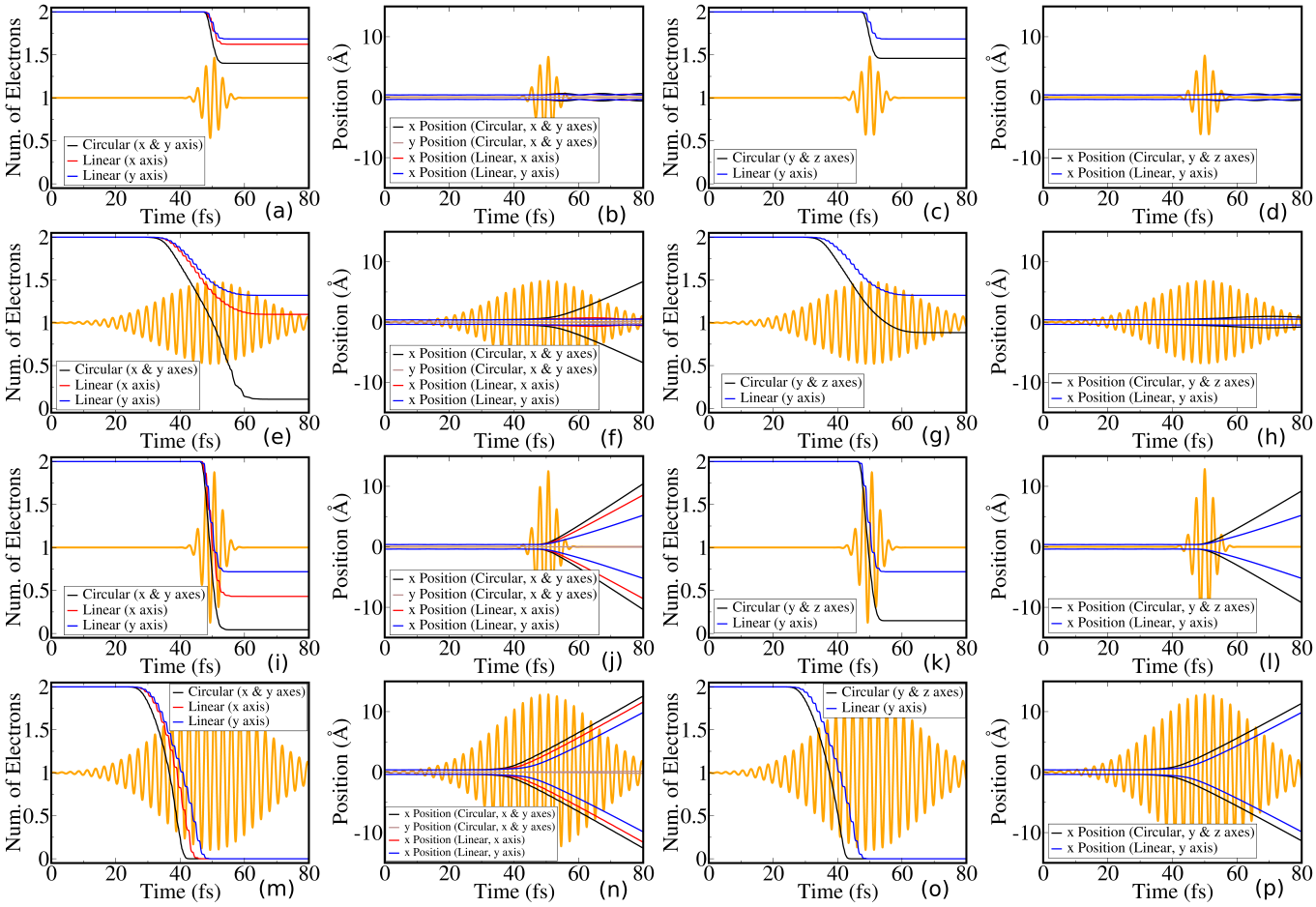

FIG. 1. (Color online) Ionization and H^+ ion positions of H_2 under the influence of a circularly polarized laser pulse. The H_2 molecule initially lies along the x axis. The circularly polarized pulse consists of two orthogonal linearly polarized pulses with a phase difference of $\frac{\pi}{2}$ between them. The polarization vectors of these composite linear pulses lie along the x and y axes in columns (1-2) and along the y and z axes in columns (3-4). Columns (1) and (3) show the total ionization of the molecule and columns (2) and (4) show the position of the H^+ ions. For comparison, in each panel the total ionization and ion positions due to a single linearly polarized pulse is shown. The wavelength of all considered pulses is 790 nm. For panels (a-h) the laser intensity is $4 \cdot 10^{14} \frac{\mathrm{W}}{\mathrm{cm}^2}$ and in panels (i-p) it is $14 \cdot 10^{14} \frac{\mathrm{W}}{\mathrm{cm}^2}$. For panels (a-d) and (i-m) the FWHM pulse width is 4.5 fs, and in panels (e-h) and (m-p) the FWHM pulse width is 25 fs.

along the y axis since, by symmetry, a linearly polarized pulse aligned along the z axis would produce the same ionization and fragmentation as one along the y axis.

As shown in Fig. 1.c, a circularly polarized laser pulse of intensity $4 \cdot 10^{14} \frac{\mathrm{W}}{\mathrm{cm}^2}$ and pulse width 4.5 fs ionizes the molecule by 0.54 electron, which is smaller than the corresponding ionization induced when the alignment of the polarization vectors lie along the x and y axes. Since the ionization is even smaller at this alignment it is unsurprising that the H-H bond remains unbroken and only a small oscillation is observed (see Fig. 1.d). The corresponding linearly polarized pulse aligned along the y axis ionizes 0.32 electron, and the ionization due to the circularly polarized pulse is smaller than the sum from two corresponding linearly polarized pulses.

At an intensity of $4 \cdot 10^{14} \frac{\mathrm{W}}{\mathrm{cm}^2}$ and a pulse width of 25 fs, the circularly polarized pulse ionizes the molecule by 1.13 electrons (see Fig. 1.g). The linearly polarized pulse ionizes 0.68 electron. No bond breaking is observed for any of the pulses (see Fig. 1.h). Hence, unlike the previous alignment, there is no enhanced ionization and the circularly polarized pulse induces less ionization than the sum from two corresponding linear pulses.

The dynamics of the remaining two pulses (Fig. 1.k and 1.o) are qualitatively quite similar for either alignment and we do not remark on them any further.

B. C_2H_2

In this section we present the simulation results for the C_2H_2 molecule. We again break down the results into two subsections according to alignment.

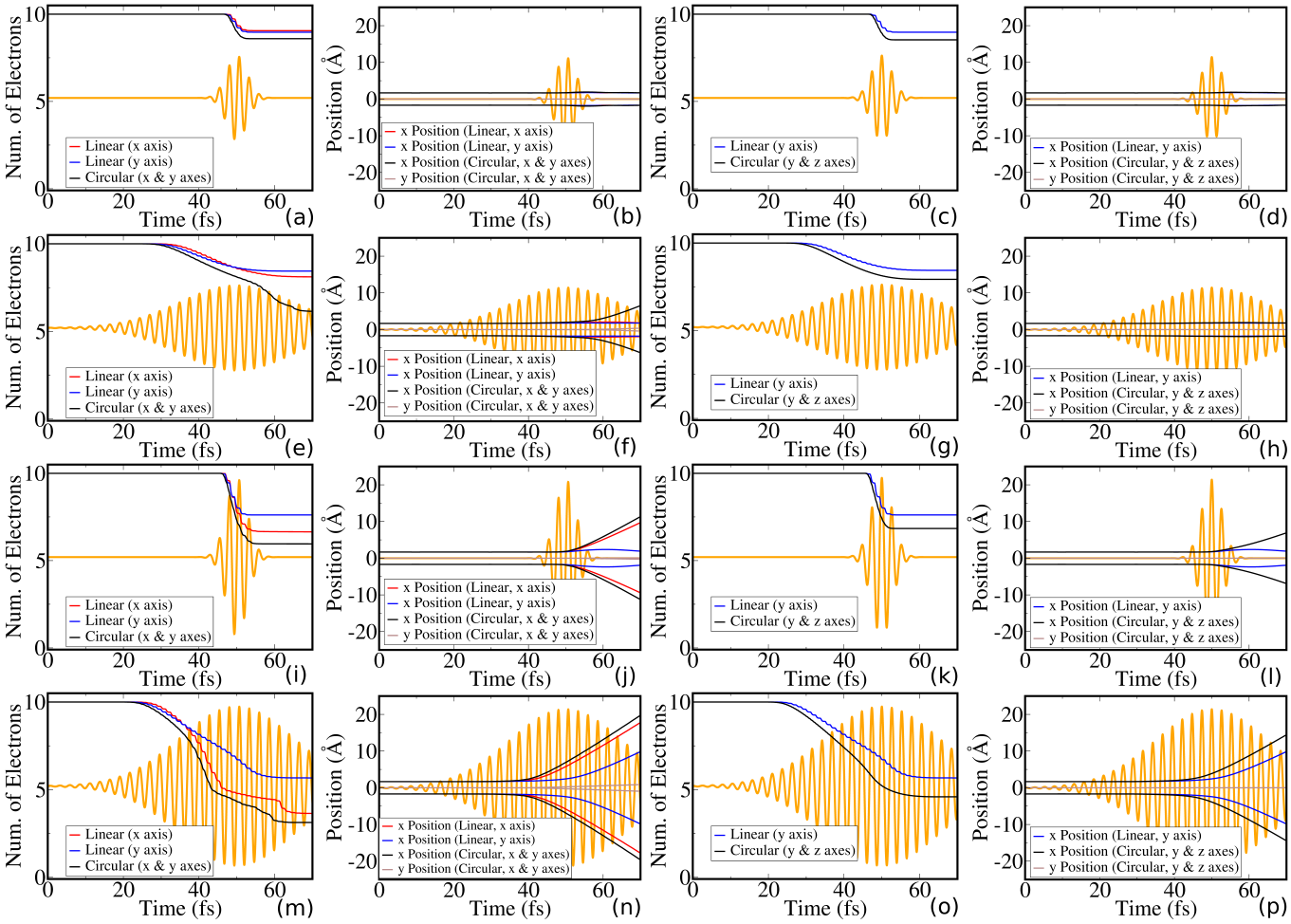

FIG. 2. (Color online) Ionization and H^+ ion positions of C_2H_2 under the influence of a circularly polarized laser pulses. The molecule initially lies along the x axis. The circularly polarized pulse consists of two orthogonal linearly polarized pulses with a phase difference of $\frac{\pi}{2}$ between them. The polarization vectors of these composite linear pulses lie along the x and y axes in columns (1-2) and along the y and z axes in columns (3-4). Columns (1) and (3) show the total ionization of the molecule, and columns (2) and (4) show the position of the H^+ ions. For comparison, in each panel the total ionization and ion positions due to a single linearly polarized pulse is shown. The wavelength of all considered pulses is 790 nm. For panels (a-h) the laser intensity is $4 \cdot 10^{14} \frac{\mathrm{W}}{\mathrm{cm}^2}$ and in panels (i-p) it is $14 \cdot 10^{14} \frac{\mathrm{W}}{\mathrm{cm}^2}$. For panels (a-d) and (i-m) the FWHM pulse width is 4.5 fs, and in panels (e-h) and (m-p) the FWHM pulse width is 25 fs.

1. *Polarization vectors along the x and y axes*

Columns (1-2) of Fig. 2 show the ionization and fragmentation dynamics of a C_2H_2 molecule driven by a circularly polarized laser pulse whose polarization vectors, $\hat{\mathbf{k_1}}$ and $\hat{\mathbf{k_2}}$, lie along the x and y axes respectively (see eq. 5). As with H_2, the linear C_2H_2 molecule initially lies along the x axis.

As shown in Fig. 2.a, a circularly polarized pulse of intensity $4 \cdot 10^{14} \frac{\mathrm{W}}{\mathrm{cm}^2}$ and pulse width 4.5 fs ionizes the molecule by 1.41 electrons. This pulse is too weak to break the C-H bond (see Fig. 2.b).A linearly polarized pulse aligned along the x axis ionizes 0.95 electron, and y axis alignment induces an ionization of 1.04 electrons, and the circularly polarized pulse induces ionization smaller than the sum from two corresponding linear pulses.

In Fig. 2.e, the intensity is $4{\cdot}10^{14} \frac{\mathrm{W}}{\mathrm{cm}^2}$ and pulse width is 25 fs. The circularly polarized pulse induces an ionization of 3.86 electrons. In this case the ionization is sufficient to cause a Coulomb explosion, and the two H^+ move apart essentially along the molecular axis (x axis) with a very small separation along the y axis (see Fig. 2.f). The corresponding linearly polarized pulses aligned along the x and y axes induce an ionization of 1.93 and 1.58 electrons, respectively, but do not induce Coulomb explosion. Just as for H_2, at this pulse strength the circularly polarized pulse benefits from enhanced ionization as the C-H bonds increase, leading to a highly efficient ionization

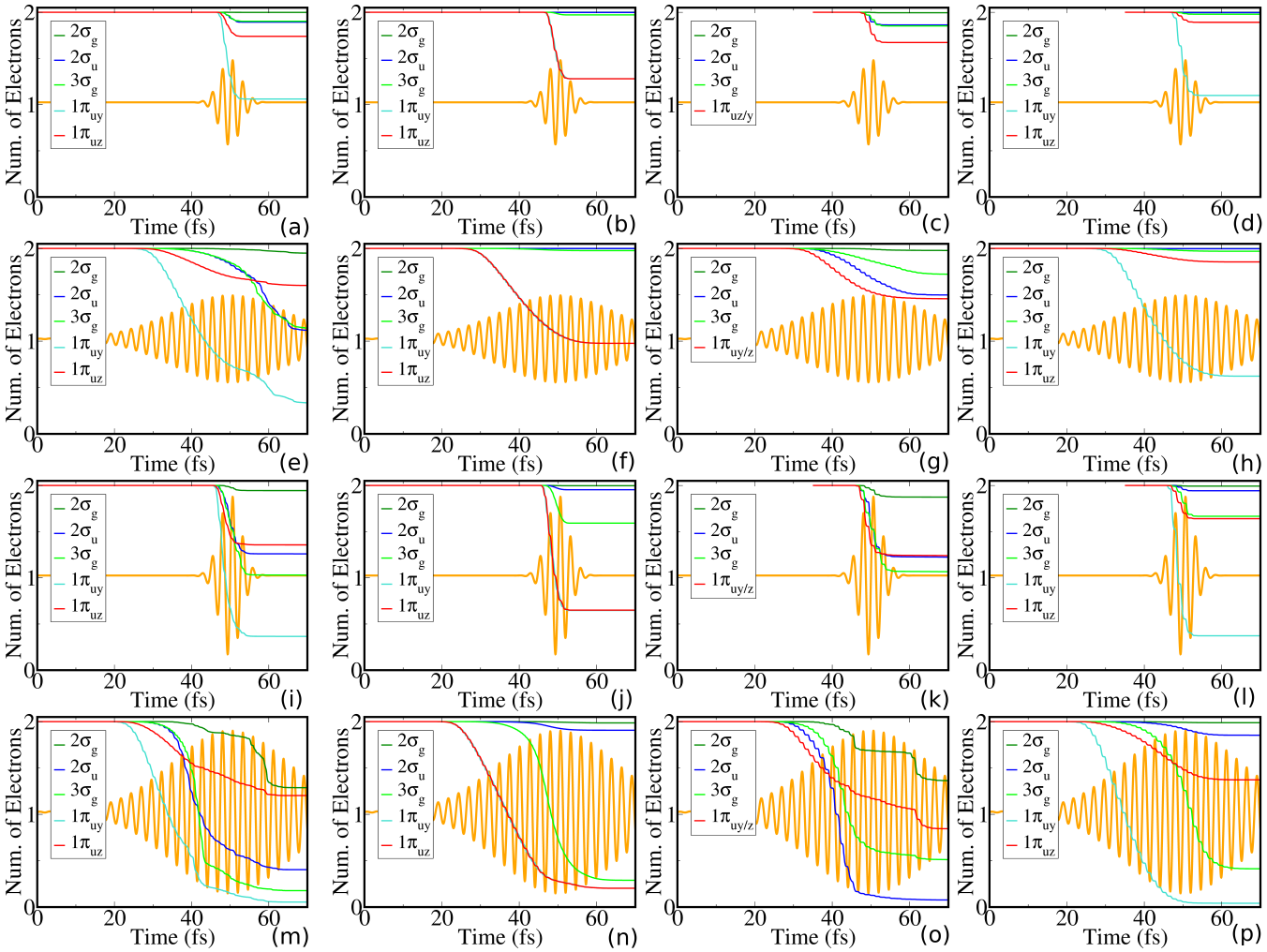

FIG. 3. (Color online) Ionization of the time-dependent Kohn-Sham orbitals of C_2H_2 under the influence of a circularly or linearly polarized laser pulse. The linear molecule initially lies along the x axis. Columns (1-2) show the orbital ionization due to a circularly polarized laser pulse, which consists of two orthogonal linearly polarized fields, which lie along the x and y axes in column (1) and along the y and z axes in column (2), with a phase difference of $\frac{\pi}{2}$ between them. For comparison, columns (3-4) show the orbital ionization due to a linear laser pulse whose polarization vector lies along the x axis in column (3) and the y axis in column (4). The wavelength of all considered pulses is 790 nm. For panels (a-h) the laser intensity is $4 \cdot 10^{14} \frac{\mathrm{W}}{\mathrm{cm}^2}$ and in panels (i-p) $14 \cdot 10^{14} \frac{\mathrm{W}}{\mathrm{cm}^2}$. For panels (a-d) and (i-m) the FWHM pulse width is 4.5 fs, and in panels (e-h) and (m-p) the FWHM pulse width is 25 fs. For ease of comparison to the other panels, the plots in panels (c),(d),(k), and (l) have been shifted such that the peak of the laser's Gaussian envelope occurs at 50 fs.

which surpasses the sum of the two individual linearly polarized pulses.

In Fig. 2.i, where the intensity is $14 \cdot 10^{14} \frac{\mathrm{W}}{\mathrm{cm}^2}$ and pulse width is 4.5 fs, a circularly polarized pulse induces an ionization of 4.07 electrons, while the corresponding linearly polarized pulses aligned along the x and y axes induce an ionization of 3.37 and 2.40 electrons, respectively. The circularly polarized pulse and the linearly polarized pulse aligned along the x axis are of sufficient strength to induce Coulomb explosion (see Fig. 2.j). When the linearly polarized pulse is aligned along the y axis the C-H bond does not break. While only the x aligned linear pulse experiences enhanced ionization, this is sufficient to insure that the ionization induced by the circularly polarized pulse is smaller than the sum of the two linearly polarized pulses.

A circularly polarized pulse with intensity $14 \cdot 10^{14} \frac{\mathrm{W}}{\mathrm{cm}^2}$ and pulse width 25 fs ionizes 6.90 electrons (see Fig. 2.m). Meanwhile corresponding linearly polarized pulses aligned along the x or y axis ionize the molecule 6.38 and 4.37 electrons, respectively. The sum of the two individual pulses would exceed 10 electrons, the total number of valence electrons, but the circularly polarized pulse induces only somewhat more ionization than just the x axis aligned linearly polarized pulse. All three pulses have sufficient strength to induce Coulomb explosion (see Fig. 2.n). For the circularly polarized pulse

there is a significant amount of motion in the y direction.

The C_2H_2 molecule has five Kohn–Sham (KS) orbitals and hence the ionization dynamics are much more complex than that of H_2, which only has one KS orbital. For the remainder of this section we consider the ionization from individual KS orbitals induced by the circularly and linearly polarized pulses.

Fig. 3.a shows the ionization of the KS orbitals induced by the circularly polarized pulse of intensity $4 \cdot 10^{14} \frac{\mathrm{W}}{\mathrm{cm}^2}$ and pulse width of 4.5 fs. The ionization due to linearly polarized pulses aligned along the x and y axes are shown in Fig. 3.c and 3.d, respectively. The orbital ionization induced by the circularly polarized pulse shares many of the features seen for the linearly polarized pulses. In particular, the ionization of most of the KS orbitals in Fig. 3.a qualitatively similar to the ionization observed in Fig. 3.c. However the circularly polarized pulse induces a very large ionization of the $1\pi_{uy}$ orbital, comparable to the ionization observed in Fig. 3.d.

Fig. 3.e shows the orbital ionization due to a circularly polarized laser pulse with intensity $4 \cdot 10^{14} \frac{\mathrm{W}}{\mathrm{cm}^2}$ and pulse width 25 fs. Interestingly, the $2\sigma_u$ and $3\sigma_g$ orbitals show a very large ionization which is not observed for either linearly polarized pulse (see Fig. 3.g and 3.h). The ionization of these two orbitals exceeds the ionization of the $1\pi_{uz}$ orbital. The $1\pi_{uz}$ orbital is one of the two highest occupied molecular orbitals (HOMO) prior to the application of the laser, which breaks the orbital's symmetry with the $1\pi_{uy}$ orbital. The increased ionization of the inner σ orbitals is indicative of an enhanced ionization mechanism, where the ionization of the inner orbitals becomes more efficient as the C-H bond length is increased [5, 33]. Indeed, as was noted above the circularly polarized pulse induces bond breaking while the individual linearly polarized pulses do not. This explains the qualitative differences in the ionization of the $2\sigma_u$ and $3\sigma_g$ orbitals.

Fig. 3.i shows the orbital ionization due to a circularly laser pulse with intensity $14 \cdot 10^{14} \frac{\mathrm{W}}{\mathrm{cm}^2}$ and pulse width 4.5 fs. Since the bond breaking and enhanced ionization occur for both the circularly polarized pulse and the linearly polarized pulse aligned along the x axis (Fig. 3.k), the ionization induced by these two pulses of the inner $2\sigma_u$ and $3\sigma_g$ orbitals are qualitatively similar.

At intensity $14 \cdot 10^{14} \frac{\mathrm{W}}{\mathrm{cm}^2}$ and pulse width 25 fs, the circularly polarized pulse and the linearly polarized pulses all induce bond breaking (see Fig. 2.m, 2.o, and 2.p). One might expect that for the circularly polarized pulse the ionization of each of the KS orbitals would be strictly greater than that of either linear pulse alone. However, the ionization of the $2\sigma_u$ and $1\pi_{uz}$ orbitals induced by the circularly polarized pulse (see Fig. 3.m) is significantly less than that of the linearly polarized pulse aligned along the x axis (see Fig. 3.o). The orbital ionization dynamics here are very complex compared to the previous cases and cannot be explained simply by either the presence or absence of enhanced ionization.

In the enhanced ionization model as is usually described [47], the C-H bond length increases to a critical separation and then the ionization proceeds instantaneously at a fixed C-H bond length. However, the ionization does not occur instantaneously and the bond length changes even as the ionization proceeds. The ionization efficiency will therefore depend on the exact trajectories of the H^+ ions. As shown in [48], the enhanced ionization mechanism affects the KS orbitals of C_2H_2 differently if the ionization occurs in a state of very large C-H bond lengths relative intermediate C-H bond lengths. For instance it was shown that for a linearly polarized pulse with polarization along the x axis, as the C-H bond length is increased from equilibrium up to about 3 Å the ionization efficiency of the $3\sigma_g$ and $2\sigma_u$ orbitals both increase and are nearly identical. However, as the bond lengths are increased further the ionization efficiency of the $3\sigma_g$ increases while the ionization efficiency of the $2\sigma_u$ decreases. Fig. 2.n shows that for the circularly polarized pulse the H^+ ions move more quickly, and therefore some fraction of the ionization time occurs while the C-H bond lengths are large. Meanwhile, for the linearly polarized pulse aligned along the x axis the ionization occurs at intermediate bond lengths. Hence the ionization of the $3\sigma_g$ is greater in Fig. 3.m than in Fig. 3.o, while the ionization of the $2\sigma_u$ is smaller. Similarly, at very large C-H bond lengths the ionization efficiency of the $1\pi_{uz}$ orbital decreases explaining why the ionization of this orbital is smaller in in Fig. 3.m than in Fig. 3.o.

2. *Polarization vectors along the y and z axes*

Columns (3-4) of Fig. 2 show the ionization and fragmentation of a C_2H_2 molecule due to a circularly polarized laser pulse whose polarization vectors, $\hat{\mathbf{k_1}}$ and $\hat{\mathbf{k_2}}$, lie along the z and y axes respectively (see eq. 5).

As shown in Fig. 2.c, a circularly polarized laser pulse of intensity $4 \cdot 10^{14} \frac{\mathrm{W}}{\mathrm{cm}^2}$ and pulse width 4.5 fs ionizes the molecule by 1.47 electrons The linearly polarized pulse pulse ionizes 1.04 electrons. Neither pulse breaks C-H bond (see Fig. 2.d and 2.h), and since enhanced ionization does not occur for either pulse the ionization of the circularly polarized pulse is smaller than the sum induced by two linearly polarized pulses of the same intensity and duration.

At an intensity of $14 \cdot 10^{14} \frac{\mathrm{W}}{\mathrm{cm}^2}$ and a pulse width of 4.5 fs, the circularly polarized pulse induces an ionization of 3.2 electrons, while the corresponding linearly polarized pulse induces an ionization of 2.40 electrons (see Fig 2.k). Only the circularly polarized pulse is sufficiently strong to induce Coulomb explosion (see Fig. 2.l). However, the bond length only increases significantly after the ionization has already completed and very little enhanced ionization occurs. Hence, the ionization of the circularly polarized pulse is much smaller than the sum of the ion-

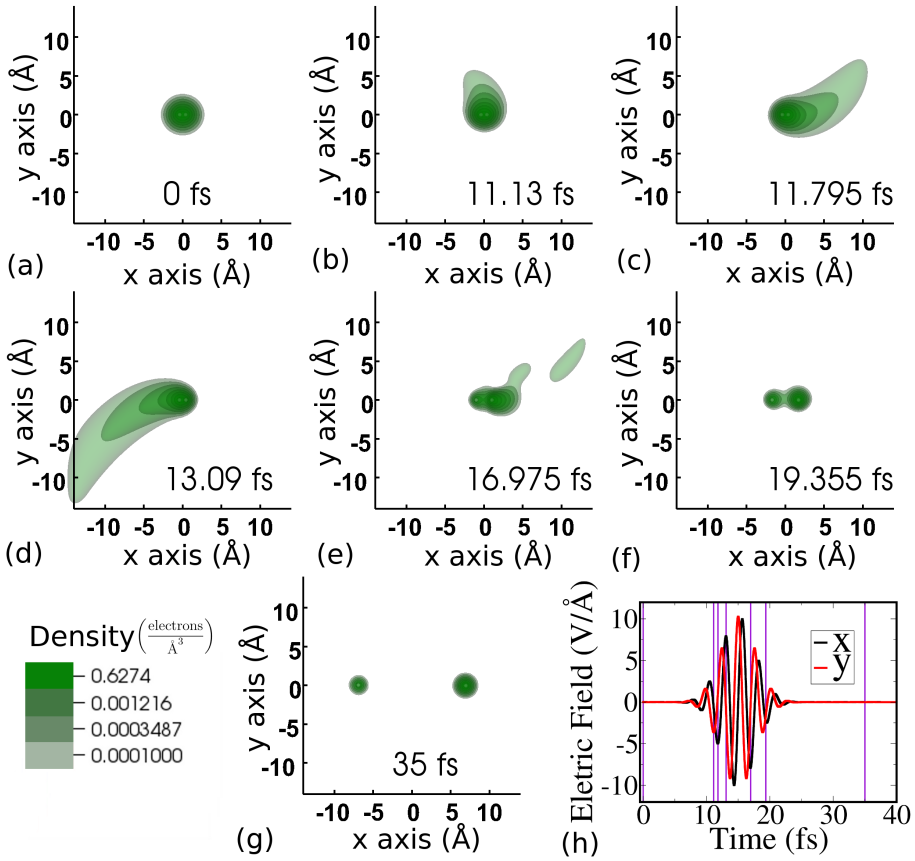

FIG. 4. (Color online) Time evolution of the electron density of H_2 subjected to a 4.5 fs pulse with a peak intensity of $14 \cdot 10^{14}$W/cm^2 which is circularly polarized with linear components along the x and y axes. The H_2 molecule initially lies along the x axis. (a-g) Snapshots of the electron density of H_2 for various times (h) Plot of the electric field of the two linear components of the circularly polarized laser pulse and of the total number of electrons. Violet vertical lines indicate the times of the snapshots in panels (a-g). The electric field of the circularly polarized pulse rotates clockwise in the $x-y$ plane. As the electric field increases the electron density develops an extended tail, indicating excitation and ionization, which rotates clockwise, lagging somewhat behind the electric field. At 16 fs the ionization rate begins to slow and the Coulomb well of the H^+ ion nearest to the tail recaptures some of the electrons. By 19 fs the electron density localized to the right H^+ ion is visibly greater than that of the left H^+ ion. The molecule dissociates more quickly than the electron density can equilibrate between the two ions, and this asymmetric charge distribution persists until the end of the simulation.

ization from two individual linearly polarized pulses.

In Fig. 2.o, the intensity is $14 \cdot 10^{14} \frac{\text{W}}{\text{cm}^2}$ and the pulse width is 25 fs. The circularly polarized pulse induces an ionization of 5.43 electrons, and the linearly polarized pulse produces an ionization of 4.37 electrons. Both the linearly polarized and circularly polarized pulses cause Coulomb explosion (see Fig. 2.p), and hence the ionization of the circularly polarized pulse is much smaller than the sum of the ionization from two individual linearly polarized pulses.

We now turn our attention to the ionization of the individual KS orbitals. Column 2 of Fig. 3 shows the ionization induced by the circularly polarized pulses and Column 4 shows the ionization due to the linearly polarized pulses with polarization aligned along the y axis. Due to the symmetry about the molecular axis, the ionization induced by linearly polarized pulses aligned along the z axis would look exactly the same except that the ionization of the $1\pi_{uz}$ and $1\pi_{uy}$ orbitals would be exchanged. Unlike the alignment presented in the previous subsection, the orbital ionization induced by the circularly polarized pulses is qualitatively very similar to the ionization induced by linearly polarized pulses of the same pulse strength. The only notable difference between the circularly and linearly polarized pulses is that the circularly polarized pulse nearly exactly preserves the symmetry between the $1\pi_{uz}$ and $1\pi_{uy}$ orbitals. The time–dependent ionization of these orbitals would be exactly identical if not for the $\frac{\pi}{2}$ phase difference between the two linearly polarized laser pulses that compose the circularly polarized pulse (eq. 5). The qualitative similarity of the orbital ionization induced by the circularly and linearly polarized pulses may be attributed to the fact that they do not induce different enhanced ionization dynamics for any of the intensities or durations considered.

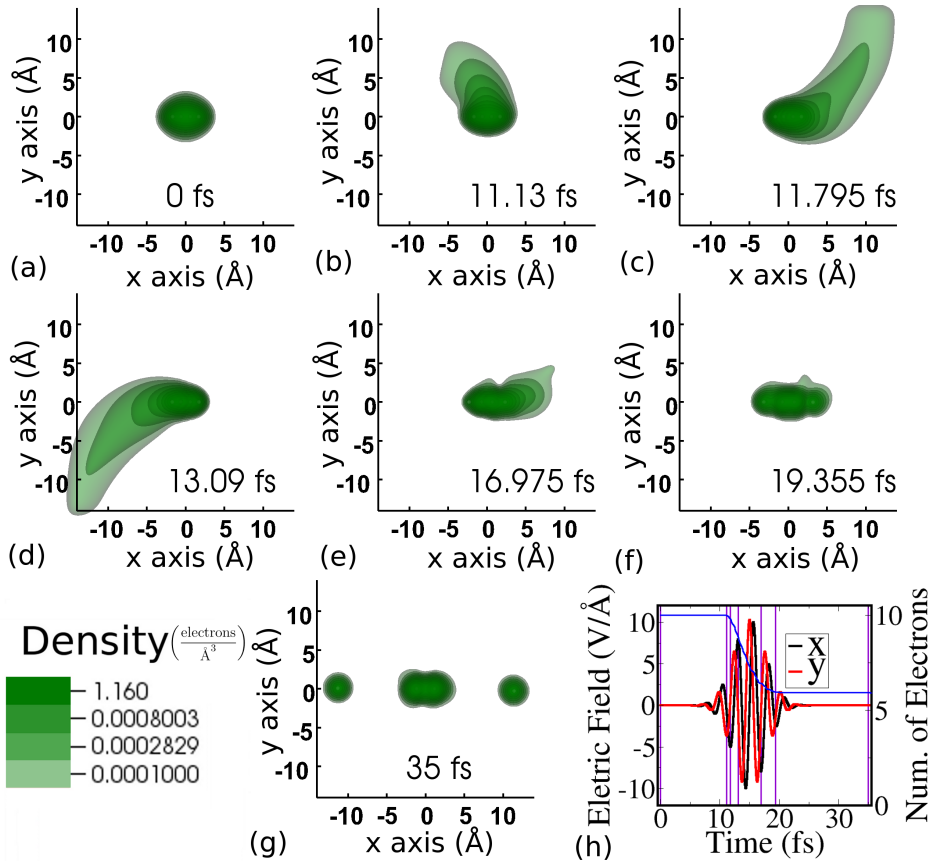

FIG. 5. (Color online) Time evolution of the electron density of C_2H_2 subjected to a 4.5 fs pulse with a peak intensity of $14 \cdot 10^{14}$W/cm^2 which is circularly polarized with linear components along the x and y axes. The molecule initially lies along the x axis. (a-g) Snapshots of the electron density of C_2H_2 for various times (h) Plot of the electric field of the two linear components of the circularly polarized laser pulse and of the total number of electrons. Violet vertical lines indicate the times of the snapshots in panels (a-g). The electric field of the circularly polarized pulse rotates clockwise in the $x-y$ plane. As the electric field increases the electron density develops an extended tail, indicating excitation and ionization, which rotates clockwise, lagging somewhat behind the electric field.

C. Discussion and Summary

The usual mechanism for nonsequential ionization driven by a linearly polarized pulse is the recollision of electrons with its parent molecule. In this model, the laser pulse first ionizes the electron from the parent molecule and then when the electric field reverses direction it drives the electron back towards its parent molecule. The recolliding electron ionizes additional electrons bound to the parent molecule.

For a circularly polarized pulse there is no reversal of the field. However recollision may occur when the electron is driven along an elliptical path which recollides with the parent molecule [49]. In particular, for a diatomic molecule an electron bound to one nucleus may be driven to the other nucleus where it collides with and ionizes an electron localized at that site. This process is dependent on the internuclear distance, R. [31]

Xie et al. [29] experimentally observed the C_2H^+/H^+ fragmentation channel of C_2H_2 induced by a circularly polarized pulses with intensity $3 \cdot 10^{14} \frac{\mathrm{W}}{\mathrm{cm}^2}$ and a linearly polarized pulse with intensity $4 \cdot 10^{14} \frac{\mathrm{W}}{\mathrm{cm}^2}$. Both pulses had sub-5fs duration. They find that the yield of high-energy fragments are suppressed for circular polarization, which is attributed to suppression of nonsequential double ionization. At higher intensities ($> 7 \cdot 10^{14} \frac{\mathrm{W}}{\mathrm{cm}^2}$ and pulse widths (> 10 fs), they find that the high energy fragments are suppressed already for linear polarization. At intensities and pulse durations where sequential ionization is probable for a linearly polarized pulse one would expect to see a suppression of the ions' kinetic energy. At $4 \cdot 10^{14} \frac{\mathrm{W}}{\mathrm{cm}^2}$ intensity and 4.5 fs pulse duration fragmentation does not occur in our simulations for either H_2 or C_2H_2 (see Fig. 1 and 2). We therefore cannot compare the ion kinetic energy due to linear and circular polarizations in the regime where nonsequential ionization is probable. At higher intensities and pulse durations, the sequential ionization regime, our simulations show that circular polarization leads to greater ion kinetic energies

as compared to linear polarization (see Fig. 1 and 2). At low intensity and pulse duration, our simulations do not show a fundamental difference in the the ionization dynamics of C_2H_2 for either circularly and linearly polarized pulses.

Wu et al. [50] employed a two-particle coincidence experiment to investigate the dynamics of the ions and electrons of H_2 under the influence of a circularly polarized pulse (35-fs, 790 nm, $1.2{\cdot}10^{14}\,\frac{\mathrm{W}}{\mathrm{cm}^2}$). They found a moderate asymmetry in the angle-resolved H^+ yield, indicating that electron localization is more probable on one nuclei than the other. In our simulations we observe a small electron localization for H_2 for the two medium strength pulses when the polarization vectors lie on the x and y axes. Fig. 4 shows dynamics of the electrons and ions for various times for the pulse with intensity $14{\cdot}10^{14}\,\frac{\mathrm{W}}{\mathrm{cm}^2}$ and pulse width 4.5 fs. By calculating the integrals $\int_{x>0}\rho\, d^3x$ and $\int_{x<0}\rho\, d^3x$ at t=35 fs, long after the ionization has completed and the molecule has dissociated, we obtain a measure of the number of electrons localized to each ion. For pulse intensity $14{\cdot}10^{14}\,\frac{\mathrm{W}}{\mathrm{cm}^2}$ and pulse width 4.5 fs, after ionization there are 0.042 electrons remaining with 0.035 electrons localized on the right H^+ ion and 0.007 electrons localized on the left H^+ ion. At intensity $4{\cdot}10^{14}\,\frac{\mathrm{W}}{\mathrm{cm}^2}$ and pulse width 25 fs, there are 0.011 electrons remaining after ionization with 0.095 electrons on the right ion and 0.011 electrons on the left ion. This moderate asymmetry is in qualitative agreement with the results of Wu et al.

Fig. 5 shows snapshots of the ionization and fragmentation of C_2H_2 for the same pulse and alignment considered in Fig. 4. The dynamics proceed similarly except in the final few panels. While the asymmetry in the electron localization is not strictly zero, the effect is much smaller compared to the H_2 molecule and cannot be distinguished by sight.

In summary, using TDDFT simulations coupled with the Ehrenfest dynamics we have presented an in depth investigation of the coupled ionization and fragmentation dynamics of H_2 and C_2H_2 for a variety of strong circularly and linearly polarized laser pulses and considered two alignments of the molecular axis relative to the laser polarization. We found that the coupled electron-ion dynamics driven by a circularly polarized pulse of sufficient strength follow the Enhanced Ionization mechanism[47, 51–54] where the pulse stretches the molecule to extended geometries and then the ionization proceeds with greater efficiency. Furthermore we found that the increased of the C-H bond lengths in acetylene leads to greater ionization efficiency of the inner $3\sigma_g$ and $2\sigma_u$ molecular orbitals, a signature of Enhanced Ionization, in qualitative agreement with the experimental findings of Gong et al. [5]. We also found that the ionization dynamics of the Kohn–Sham orbitals in C_2H_2 depend on the rate at which the C-H bond length increases. Finally, we found that a circularly polarized pulse leads to moderate asymmetric electron localization in the fragmented H_2 molecule, in qualitative agreement with the results of Wu et al.[50]. The present work investigated the interaction of small linear molecules and strong short laser pulses and capture many of the features of interactions with more general molecules. Topics for future work include an investigation of nonlinear or large molecules. The predictions of the present work may be used to motivate future experiments which consider the effects of aligned molecules interacting with strong fields.

[1] B. Manschwetus, T. Nubbemeyer, K. Gorling, G. Steinmeyer, U. Eichmann, H. Rottke, and W. Sandner, Phys. Rev. Lett. **102**, 113002 (2009).

[2] P. von den Hoff, I. Znakovskaya, M. F. Kling, and R. de Vivie-Riedle, Chem. Phys. **366**, 139 (2009).

[3] G. Sansone, F. Kelkensberg, J. F. Perez-Torres, F. Morales, M. F. Kling, W. Siu, O. Ghafur, P. Johnsson, M. Swoboda, E. Benedetti, F. Ferrari, F. Lepine, J. L. Sanz-Vicario, S. Zherebtsov, I. Znakovskaya, A. L'Huillier, M. Y. Ivanov, M. Nisoli, F. Martin, and M. J. J. Vrakking, Nature (London) **465**, 763 (2010).

[4] I. Bocharova, R. Karimi, E. F. Penka, J.-P. Brichta, P. Lassonde, X. Fu, J.-C. Kieffer, A. D. Bandrauk, I. Litvinyuk, J. Sanderson, and F. Légaré, Phys. Rev. Lett. **107**, 063201 (2011).

[5] X. Gong, Q. Song, Q. Ji, H. Pan, J. Ding, J. Wu, and H. Zeng, Phys. Rev. Lett. **112**, 243001 (2014).

[6] F. Krausz and M. Ivanov, Rev. Mod. Phys. **81**, 163 (2009).

[7] W. Li, X. Zhou, R. Lock, S. Patchkovskii, A. Stolow, H. C. Kapteyn, and M. M. Murnane, Science **322**, 1207 (2008).

[8] S. Haessler, J. Caillat, W. Boutu, C. Giovanetti-Teixeira, T. Ruchon, T. Auguste, Z. Diveki, P. Breger, A. Maquet, B. Carré, R. Taïeb, and P. Salières, Nature Photon. **6**, 200 (2010).

[9] Z. Chang, A. Rundquist, H. Wang, M. M. Murnane, and H. C. Kapteyn, Phys. Rev. Lett. **79**, 2967 (1997).

[10] B. K. McFarland, J. P. Farrell, P. H. Bucksbaum, and M. Ghr, Science **322**, 1232 (2008), http://www.sciencemag.org/content/322/5905/1232.full.pdf.

[11] K.-J. Yuan and A. D. Bandrauk, Phys. Rev. A **81**, 063412 (2010).

[12] C. Brif, R. Chakrabarti, and H. Rabitz, New J. Phys. **12**, 075008 (2010).

[13] K. Krieger, A. Castro, and E. K. U. Gross, Chem. Phys. **391**, 50 (2011).

[14] M. Shapiro and P. Brumer, *Quantum Control of Molecular Processes* (Wiley-VCH, Weinheim, 2012).

[15] A. N. Pfeiffer, C. Cirelli, M. Smolarski, R. Dorner, and U. Keller, Nat Phys **7**, 428 (2011).

[16] Y. Zhou, C. Huang, Q. Liao, and P. Lu, Phys. Rev. Lett.

109, 053004 (2012).
[17] W. Becker and H. Rottke, Contemp. Phys. **49**, 199 (2008).
[18] R. Dörner, T. Weber, M. Weckenbrock, A. Staudte, M. Hattass, R. Moshammer, J. Ullrich, and H. Schmidt-Bocking, Advances in Atomic Molecular and Optical Physics **48**, 1 (2002).
[19] B. Walker, B. Sheehy, L. F. DiMauro, P. Agostini, K. J. Schafer, and K. C. Kulander, Phys. Rev. Lett. **73**, 1227 (1994).
[20] B. Walker, E. Mevel, B. Yang, P. Breger, J. P. Chambaret, A. Antonetti, L. F. DiMauro, and P. Agostini, Phys. Rev. A **48**, R894 (1993).
[21] D. N. Fittinghoff, P. R. Bolton, B. Chang, and K. C. Kulander, Phys. Rev. Lett. **69**, 2642 (1992).
[22] M. V. Ammosov, N. B. Delone, and V. P. Krainov, Sov. Phys. JETP **64**, 1191 (1986).
[23] X. M. Tong, Z. X. Zhao, and C. D. Lin, Phys. Rev. A **66**, 033402 (2002).
[24] K. Codling, L. J. Frasinski, and P. A. Hatherly, J. Phys. B **22**, L321 (1989).
[25] D. Dimitrovski, C. P. J. Martiny, and L. B. Madsen, Phys. Rev. A **82**, 053404 (2010).
[26] W. Becker, X. Liu, P. J. Ho, and J. H. Eberly, Rev. Mod. Phys. **84**, 1011 (2012).
[27] P. B. Corkum, Phys. Rev. Lett. **71**, 1994 (1993).
[28] P. B. Corkum, Phys. Today **64**, 36 (2011).
[29] X. Xie, K. Doblhoff-Dier, H. Xu, S. Roither, M. S. Schöffler, D. Kartashov, S. Erattupuzha, T. Rathje, G. G. Paulus, K. Yamanouchi, A. Baltuška, S. Gräfe, and M. Kitzler, Phys. Rev. Lett. **112**, 163003 (2014).
[30] C. Guo, M. Li, J. P. Nibarger, and G. N. Gibson, Phys. Rev. A **58**, R4271 (1998).
[31] A. Tong, Y. Zhou, C. Huang, and P. Lu, The Journal of Chemical Physics **139**, 074308 (2013).
[32] X. Ren, J. Zhang, P. Liu, Y. Wang, and Z. Xu, Phys. Rev. A **78**, 043411 (2008).
[33] A. Russakoff, S. Bubin, X. Xie, S. Erattupuzha, M. Kitzler, and K. Varga, Phys. Rev. A **91**, 023422 (2015).
[34] K.-J. Yuan and A. D. Bandrauk, Journal of Physics B: Atomic, Molecular and Optical Physics **45**, 105601 (2012).
[35] A. Staudte, S. Patchkovskii, D. Pavičić, H. Akagi, O. Smirnova, D. Zeidler, M. Meckel, D. M. Villeneuve, R. Dörner, M. Y. Ivanov, and P. B. Corkum, Phys. Rev. Lett. **102**, 033004 (2009).
[36] P. B. Corkum, N. H. Burnett, and F. Brunel, Phys. Rev. Lett. **62**, 1259 (1989).
[37] M. Odenweller, N. Takemoto, A. Vredenborg, K. Cole, K. Pahl, J. Titze, L. P. H. Schmidt, T. Jahnke, R. Dörner, and A. Becker, Phys. Rev. Lett. **107**, 143004 (2011).
[38] M. Odenweller, J. Lower, K. Pahl, M. Schütt, J. Wu, K. Cole, A. Vredenborg, L. P. Schmidt, N. Neumann, J. Titze, T. Jahnke, M. Meckel, M. Kunitski, T. Havermeier, S. Voss, M. Schöffler, H. Sann, J. Voigtsberger, H. Schmidt-Böcking, and R. Dörner, Phys. Rev. A **89**, 013424 (2014).
[39] A. D. Bandrauk and H. Lu, Journal of Molecular Structure: THEOCHEM **547**, 97 (2001).
[40] E. Runge and E. K. U. Gross, Phys. Rev. Lett. **52**, 997 (1984).
[41] N. Troullier and J. L. Martins, Phys. Rev. B **43**, 1993 (1991).
[42] J. P. Perdew and A. Zunger, Phys. Rev. B **23**, 5048 (1981).
[43] A. Castro, M. A. L. Marques, and A. Rubio, The Journal of Chemical Physics **121**, 3425 (2004).
[44] D. E. Manolopoulos, J. Chem. Phys. **117**, 9552 (2002).
[45] P. Ehrenfest, Z. Phys. **45**, 455 (1927).
[46] P. J. Linstrom and W. G. Mallard, eds., *NIST Chemistry WebBook, NIST Standard Reference Database Number 69* (National Institute of Standards and Technology, Gaithersburg MD, 20899, 2001).
[47] D. M. Villeneuve, M. Y. Ivanov, and P. B. Corkum, Phys. Rev. A **54**, 736 (1996).
[48] A. Russakoff, This work is still in preparation for publication.
[49] X. Wang and J. H. Eberly, New Journal of Physics **12**, 093047 (2010).
[50] J. Wu, M. Magrakvelidze, L. P. H. Schmidt, M. Kunitski, T. Pfeifer, M. Schöffler, M. Pitzer, M. Richter, S. Voss, H. Sann, H. Kim, J. Lower, T. Jahnke, A. Czasch, U. Thumm, and R. Dörner, Nat Commun **4** (2013), article.
[51] T. Seideman, M. Y. Ivanov, and P. B. Corkum, Phys. Rev. Lett. **75**, 2819 (1995).
[52] T. Zuo and A. D. Bandrauk, Phys. Rev. A **52**, R2511 (1995).
[53] S. Roither, X. Xie, D. Kartashov, L. Zhang, M. Schöffler, H. Xu, A. Iwasaki, T. Okino, K. Yamanouchi, A. Baltuska, and M. Kitzler, Phys. Rev. Lett. **106**, 163001 (2011).
[54] X. Xie, S. Roither, M. Schöffler, H. Xu, S. Bubin, E. Lötstedt, S. Erattuphuza, A. Iwasaki, D. Kartashov, K. Varga, G. G. Paulus, A. Baltuška, K. Yamanouchi, and M. Kitzler, Phys. Rev. A **89**, 023429 (2014).